 CMES, vol.15, no.1, pp.41-48, 2006

Accurate Force Evaluation for Industrial Magnetostatics Applications with Fast Bem-Fem Approaches

A. Frangi[1] **and L. Ghezzi, P. Faure-Ragani**[2]

Abstract: Three dimensional magneto-mechanical problems at low frequency are addressed by means of a coupled fast Boundary Element - Finite Element approach with total scalar potential and focusing especially on the issue of global force calculation on movable ferromagnetic parts. The differentiation of co-energy in this framework and the use of Maxwell tensor are critically discussed and the intrinsic links are put in evidence. Three examples of academic and industrial applications are employed for validation.

keyword: BEM-FEM, Magnetostatics, Material derivatives, Global force computation.

1 Introduction

Several industrial relays working at low frequency display non-linear material behaviour of fixed and movable ferromagnetic parts embedded in the linear air domain. These features naturally call for the application of coupled BEM-FEM approaches which have been discussed in several contributions (e.g. Bossavit (1998); Frangi, Faure-Ragani, and Ghezzi (2005); Kuhn (1998); Kuhn and Steinbach (2002); Springhetti, Novati, and Margonari (2006)) and take advantage of the versatility of the FEM to model material non-linearities and of the ability of integral approaches to account for infinite domains and movable structures. As often occurs in magnetostatics, the total scalar potential approach is privileged, since it is generally more robust than alternative edge element formulations (Bossavit (1998)) and avoids cancellation errors which are intrinsic in the perturbation scalar potential approach.

One of the main goals of numerical analyses is the evaluation of forces and moments which govern the mechanical response of the relay. Generally, the methods for force calculation in low frequency devices are based on one of two approaches (see e.g. Coulomb (1983); Coulomb and Meunier (1984); Henrotte, Sande, Delige, and Hameyer (2004); Kim, Lowther, and Sykulski (2005); Ren (1994); Melkebeek (2001)): the Maxwell stress tensor (MST) and the differentiation of the co-energy functional (DCF), or virtual work principle. These two approaches are usually derived from somewhat different starting points, even if in Henrotte, Sande, Delige, and Hameyer (2004); Kim, Lowther, and Sykulski (2005) their strong connection has been put in evidence employing concepts of material differentiations. This common link is here re-established in the case of a general non linear material surrounded by air in the context of the coupled BEM-FEM approach. In the MST the force is computed by integrating over a surface enclosing the volume of interest provided it does not intersect other regions with surface or volume currents. Clearly, the quality of the solution strongly depends on the choice of the surface. Virtual work, on the other hand, computes the force on a body by evaluating the variation of the co-energy of the system either by sensitivity analysis, or by imposing a small physical displacement and using finite differences. After briefly reviewing the formulation adopted in Section 2, the different approaches for computing global forces are presented in Section 3 in a unified framework and numerical examples are presented to validate the techniques proposed.

2 Formulation

Let us assume that the variation of currents inside the conductor is slow enough to neglect dynamic effects and justify the adoption of a magnetostatic formulation.

Let Ω_F denote the ferromagnetic domains, Ω_A the infinite "air" domain surrounding Ω_F and Γ the interface between Ω_F and Ω_A, endowed with the unit normal $\mathbf{n}$ pointing from Ω_F to Ω_A.

The field variables are assumed to satisfy the isotropic

[1] Politecnico di Milano, Milan, Italy.
[2] ABB AT Italy Simulation Group, Italy.

nonlinear constitutive relations:

$$\begin{aligned} &\mathbf{B}_F = \mu_r(\mathbf{x},|\mathbf{H}|)\mu_0\mathbf{H}_F \quad \text{in} \quad \Omega_F, \\ &\mathbf{B}_A = \mu_0\mathbf{H}_A \quad \text{in} \quad \Omega_A \end{aligned} \tag{1}$$

where $\mathbf{H}$ is the magnetic field intensity and $\mathbf{B}$ the magnetic flux density. Also, the current density $\mathbf{j}$ is assumed to vanish in Ω_F while currents in Ω_A are treated as input data. The governing equations are:

$$\begin{aligned} &\nabla\cdot(\mu_r\mathbf{H}_F) = 0 \quad \text{in} \quad \Omega_F, \\ &\nabla\cdot\mathbf{H}_A = 0 \quad \text{in} \quad \Omega_A \end{aligned} \tag{2}$$

$$\begin{aligned} &\nabla\wedge\mathbf{H}_F = 0 \quad \text{in} \quad \Omega_F, \\ &\nabla\wedge\mathbf{H}_A = \mathbf{j} \quad \text{in} \quad \Omega_A \end{aligned} \tag{3}$$

$$\begin{aligned} &\mathbf{B}_F\cdot\mathbf{n} = \mathbf{B}_A\cdot\mathbf{n} \quad \text{on} \quad \Gamma \\ &\mathbf{H}_F\wedge\mathbf{n} = \mathbf{H}_A\wedge\mathbf{n} \quad \text{on} \quad \Gamma \end{aligned} \tag{4}$$

Using the scalar potential approach $\mathbf{H}_F = \nabla\phi$ in Ω_F, with ϕ total scalar magnetic potential, while in Ω_A $\mathbf{H}_A = \nabla\phi^p + \mathbf{H}^a$, with ϕ^p perturbation scalar magnetic potential. $\mathbf{H}^a$ is the magnetic field computed analytically from the given currents $\mathbf{j}$ in Ω_A via Biot-Savart law.

From eqn. (4) the following interface continuity condition holds for each connected surface of the problem:

$$\nabla\phi\wedge\mathbf{n} = \nabla\phi^p\wedge\mathbf{n} + \mathbf{H}^a\wedge\mathbf{n}$$

and hence:

$$\begin{aligned} \phi(\mathbf{y}) &= \phi^p(\mathbf{y}) + \int_{\mathcal{L}} \mathbf{H}^a\cdot\boldsymbol{\tau}\,\mathrm{d}s + \phi^a(\mathbf{x}_C) \\ &= \phi^p(\mathbf{y}) + \phi^a(\mathbf{y}) \end{aligned} \tag{5}$$

where, under certain constraints which are analysed in Section 2.2, $\mathcal{L}$ is an arbitrary curve (of tangent unit vector $\boldsymbol{\tau}$) lying on Γ and starting from the arbitrary point $\mathbf{x}_C$.

A Finite Element discretization is envisaged for Ω_F based on the variational equation:

$$\begin{aligned} &\int_{\Omega_F} \nabla\tilde{\phi}(\mathbf{x})\,\mu_r(\mathbf{x},|\nabla\phi|)\nabla\phi(\mathbf{x})\mathrm{d}V \\ &\quad = \int_\Gamma \tilde{\phi}(\mathbf{x})B_n(\mathbf{x})\mathrm{d}S, \quad \forall\tilde{\phi}\in H^1(\Omega_F) \end{aligned} \tag{6}$$

where $B_n = \mathbf{B}\cdot\mathbf{n}$, while collocation BE are employed for Ω_A in view of its linear constitutive behaviour. The third Green identity written for a source point $\mathbf{y}$ lying on Γ reads:

$$\begin{aligned} k\phi^p(\mathbf{y}) = \int_\Gamma \big\{ &-G(\mathbf{y},\mathbf{x})B_n(\mathbf{x}) \\ &+ [\nabla G(\mathbf{y},\mathbf{x})\cdot\mathbf{n}(\mathbf{x})]\,\phi^p(\mathbf{x})\big\}\mathrm{d}S \end{aligned} \tag{7}$$

where kernel $G(\mathbf{y},\mathbf{x})$ is the potential theory Kelvin kernel:

$$G(\mathbf{y},\mathbf{x}) = \frac{1}{4\pi}\frac{1}{r} \qquad \text{with} \quad r = |\mathbf{x}-\mathbf{y}|$$

k depends on the geometry of Γ at $\mathbf{y}$ ($k = 1/2$ for a "smooth" surface) and ∇G denotes the gradient w.r.t. $\mathbf{x}$. Taking account of eqn. (5), eqns. (6) and (7) are expressed in terms of the unknown fields B_n and ϕ.

2.1 Numerical implementation

For the numerical solution of the above system, Ω_F is discretized with four-node tetrahedra and the set of their facets lying on Γ represents the triangulation employed for the discretization of the BEM equation (7). The total potential ϕ is chosen in the space of continuous piecewise linear functions as well as $\tilde{\phi}$, since a Galerkin approach is adopted for the FEM equations. The normal flux B_n is modeled as piecewise constant (constant over each BEM). Equation (7) is then collocated at the center of every triangular facet. Alternative elegant variational approaches have been proposed in the literature (Kuhn (1998); Kuhn and Steinbach (2002)), but collocation is adopted here in order to privilege the crucial computing speed.

The solution of the linear system is performed via an iterative GMRES solver and the matrix vector product required at each iteration is accelerated via fast multipole techniques (Greengard and Rokhlin (1997); Chew, Song, Cui, Velamparambil, Hastriter, and Hu (2004)). In Frangi, Faure-Ragani, and Ghezzi (2005) a multigrid approach was used for solving very large problems; here, on the contrary, we tackle medium size analyses like those presented in Section 4.3 and the best performances were obtained using an "implicit" condensation. The normal fluxes B_n are chosen as primary unknowns. In principle the nodal values of ϕ could be condensed out of the system, but an explicit condensation is not viable and is here replaced, at each iteration, by the following procedure. Given the present estimate of B_n, eqn. (6) is solved

for ϕ and the result is substituted back in eqn. (7) for evaluating the residuum. Since all the problems tested converge very rapidly (less than $\simeq 50$ iterations), this choice drastically reduces computing time w.r.t. to explicit condensation and yields far better performances with respect to other preconditioners tested.

2.2 *Computation of* ϕ^a

Let Γ be the union of several simply connected surfaces. For each of these surfaces, say S, we assume that a single valued ϕ^a exist on S such that $\nabla\phi^a = \mathbf{H}^a$. This requires that any closed loop that can be initially traced on S can also be continuously contracted to a single point without "cutting" a region with $\mathbf{j} \neq \mathbf{0}$. All the topologies of interest for the present investigation respect this condition, but it is worth stressing that the general situation could be addressed with the same technique at the cost of introducing suitable cuts in Ω_F with associated jump conditions for ϕ. The evaluation of ϕ^a is performed exploiting the surface spanning tree technique of common usage in edge element approaches (e.g. Biro, Preis, and Richter (1998)). Let us assume that S has been discretized with flat triangles. A spanning tree is a set of edges (of the triangles) which does not contain any closed loop and which connects all the nodes of the surface mesh. A node is selected as the root and ϕ^a is arbitrarily set to zero there. Then $\mathbf{H}^a$ is integrated numerically (or analytically) along each edge of the spanning tree. Since this line integral represents the difference between the two values at the nodes connected by the edge, all the nodal values of $\boldsymbol{\phi}^a$ can readily be computed. The field interpolated with linear shape functions from these nodal values is an exact potential.

3 Computation of global forces

In industrial applications like the circuit breaker of Section 4.3, one of the main objectives of the analysis is the computation of forces and moments acting on the movable ferromagnetic part Ω_{FM} which can be often treated as rigid. This poses severe difficulties especially when the gap between Ω_{FM} and the other fixed ferromagnetic parts Ω_{FF} is much smaller than the typical problem dimension. One of the key advantages of a coupled BEM-FEM approach is that Ω_{FM} can be freely moved without having to modify the mesh or deform it, hence it is the ideal tool for the problem at hand.

In the literature on Finite Elements several techniques are proposed resorting either to the concept of Maxwell tensor or to the differentiation of the co-energy functional. These techniques are here revisited to discuss their applicability in the present context.

Let us consider the infinite domain containing the structure of interest in which the movable part Ω_{FM} undergoes a given rigid body movement. We continuously extend the movement to the surrounding air by means of the mapping $\mathbf{y} = \boldsymbol{\Phi}(\mathbf{x},t)$, with initial condition $\mathbf{x} = \boldsymbol{\Phi}(\mathbf{x},0)$, which defines a domain transformation as a function of a parameter t (fictitious time) and initial position $\mathbf{x}$. We will also assume that one can identify a surface S_Φ in air such that: i) S_Φ encloses completely Ω_{FM} and $\mathbf{x} = \boldsymbol{\Phi}(\mathbf{x},t)$ (i.e. no displacements) on S_Φ and outside it (in particular on fixed ferromagnetic parts); ii) the surface S_Φ does not enclose or cut conductors ($\mathbf{j} = \mathbf{0}$ inside S_Φ).

The transformation $\boldsymbol{\Phi}(\mathbf{x},t)$ induces the velocity $\boldsymbol{\theta}(\mathbf{y},t) = \boldsymbol{\Phi}_{,t}(\mathbf{x},t)$ which, in Ω_{FM}, will necessarily have the rigid-body form:

$$\boldsymbol{\theta}(\mathbf{y},t) = \mathbf{d}(t) + \boldsymbol{\omega}(t) \wedge (\mathbf{y} - \mathbf{x}_0)$$

where $\mathbf{d}(t)$ represents the velocity of $\mathbf{x}_0$, $\boldsymbol{\omega}(t)$ the angular velocity associated to the rigid body movement and $\mathbf{x}_0$ is a fixed arbitrary point.

The instant power of magnetic forces will then have the simple expression:

$$P(t) = \mathbf{F}(t) \cdot \mathbf{d}(t) + \mathbf{C}(\mathbf{x}_0,t) \cdot \boldsymbol{\omega}(t) \tag{8}$$

where $\mathbf{F}(t)$ and $\mathbf{C}(\mathbf{x}_0,t)$ are the resultant force and resultant moment with respect to $\mathbf{x}_0$, respectively, of forces acting on Ω_{FM}.

3.1 *Direct differentiation of co-energy*

Let us now focus the attention on the co-energy functional

$$\Psi = \int_{\Omega_\infty} \int_0^{\mathbf{H}} \mathbf{B} \mathrm{d}\mathbf{H} \mathrm{d}V \tag{9}$$

It is well known that the instant power $P(t)$ associated to the rigid body movement of Ω_{FM} is the material derivative $\overset{\star}{\Psi}$ (see e.g. Coulomb (1983); Coulomb and Meunier (1984); Henrotte, Sande, Delige, and Hameyer (2004); Kim, Lowther, and Sykulski (2005)) of Ψ when the material derivatives $\overset{\star}{\phi}$ of ϕ in the ferromagnetic parts and

$\overset{\star}{\phi}^p$ of ϕ^p in air vanish. Using the formulas of material derivatives (Appendix A:) one obtains

$$P(t) = \int_{\Omega_\infty} \mathbf{B}\overset{\star}{\mathbf{H}} \mathrm{d}V + \int_{\Omega_\infty} \left(\int_0^{\mathbf{H}} \mathbf{B} \mathrm{d}\mathbf{H} \right) \nabla\cdot\boldsymbol{\theta}\, \mathrm{d}V \tag{10}$$

The combined use of eqns. (10) and (8) with suitable choices of $\mathbf{d}$ and $\boldsymbol{\omega}$ yields the desired values of $\mathbf{F}(t)$ and $\mathbf{C}(\mathbf{x}_0, t)$.

Let us now focus on eqn. (10). In Ω_{FM} $\nabla\cdot\boldsymbol{\theta} = 0$ since the movement is rigid; moreover, $\mathbf{B}\overset{\star}{\mathbf{H}} = -\mu(\nabla\phi\cdot\nabla\boldsymbol{\theta})\cdot\nabla\phi$ and this term also vanishes for any rigid body movement. Outside S_Φ, $\boldsymbol{\theta} = 0$ by hypothesis. Moreover $\overset{\star}{\mathbf{H}}$ vanishes since it is a linear function of $\overset{\star}{\phi}$ in Ω_{FF} and of $\overset{\star}{\phi}^p$ in air, and they both vanish by hypothesis. Hence, the only contribution stems from the integration over the air region $\Delta\Omega$ between S_Φ and $\partial\Omega_{FM}$:

$$\begin{aligned} P &= \mu_0 \int_{\Delta\Omega} \left(-\mathbf{H}\cdot\nabla\boldsymbol{\theta}\cdot\mathbf{H} + \frac{1}{2}|\mathbf{H}|^2 \nabla\cdot\boldsymbol{\theta} \right) \mathrm{d}V \\ &= \int_{\Delta\Omega} \nabla\boldsymbol{\theta} : \left(-\mathbf{B}\otimes\mathbf{H} + \frac{1}{2}(\mathbf{H}\cdot\mathbf{B})\mathbb{1} \right) \mathrm{d}V \end{aligned} \tag{11}$$

This formula, often adopted in FEM approaches, requires a volume integration in $\Delta\Omega$ which is not meshed in the BEM-FEM technique and hence does not represent an appealing procedure herein.

3.2 Maxwell tensor

Considering that $\boldsymbol{\theta} = \mathbf{0}$ on S_ϕ and that no current sources are present in $\Delta\Omega$ by hypothesis, and hence $\mathbf{H} = \nabla\phi$, integrating by parts one obtains:

$$P = \int_{\partial\Omega_{FM}} \left(\mathbf{H}B_n - \frac{1}{2}(\mathbf{B}\cdot\mathbf{H})\mathbf{n} \right) \cdot\boldsymbol{\theta}\mathrm{d}S \tag{12}$$

and the vector in parenthesis is the contraction of the Maxwell tensor with the normal vector $\mathbf{n}$. The Maxwell tensor is continuous across $\partial\Omega_{FM}$, so that the power is well defined and one obtains:

$$\mathbf{F}(t) = \int_{\partial\Omega_{FM}} \left(\mathbf{H}_t B_n + \frac{1}{2}\left(\frac{1}{\mu_0}B_n^2 - \mu_0|\mathbf{H}_t|^2\right)\mathbf{n} \right) \mathrm{d}S \tag{13}$$

$$\mathbf{C}(\mathbf{x}_0, t) = \int_{\partial\Omega_{FM}} (\mathbf{y}-\mathbf{x}_0) \wedge \left(\mathbf{H}_t B_n + \frac{1}{2}\left(\frac{1}{\mu_0}B_n^2 - \mu_0|\mathbf{H}_t|^2\right)\mathbf{n} \right) \mathrm{d}S \tag{14}$$

The application of eqns. (13) and (14) is straightforward, since it can be expressed in terms of the direct unknowns ϕ and B_n. Unfortunately it is not very accurate, in general, as often remarked in the literature and commented in the sequel. However, exploiting the fact that the Maxwell tensor is divergence free if $\mathbf{j} = \mathbf{0}$, we also have:

$$\mathbf{F}(t) = \int_{S_M} \left(\mathbf{H}_t B_n + \frac{1}{2}\left(\frac{1}{\mu_0}B_n^2 - \mu_0|\mathbf{H}_t|^2\right)\mathbf{n} \right) \mathrm{d}S \tag{15}$$

$$\mathbf{C}(\mathbf{x}_0, t) = \int_{S_M} (\mathbf{y}-\mathbf{x}_0) \wedge \left(\mathbf{H}_t B_n + \frac{1}{2}\left(\frac{1}{\mu_0}B_n^2 - \mu_0|\mathbf{H}_t|^2\right)\mathbf{n} \right) \mathrm{d}S \tag{16}$$

where S_M is any surface completely contained in $\Delta\Omega$. The application of eqns. (15) and (16) requires the computation of B_n and $\mathbf{H}_t$ on S_M but is in general more reliable than eqns. (13) and (14).

One possible reason is that $\mathbf{H}_t$ in eqns. (13) and (14) is obtained by differentiating the scalar potential and hence is not as accurate as the direct BEM fields; more importantly, the currents, which are physically concentrated on the surface in the real case, appear to be smeared out by the numerical model over a solid region which has approximately the size of the elements employed in the discretization. These currents must be accounted for in order to recover the correct forces.

Experimentally, it has been remarked that "optimal" results can be be obtained if S_M is placed at a distance from $\partial\Omega_{FM}$ approximately equal to the characteristic mesh size. The shortcoming of this approach is that, especially when gaps are very narrow, the construction of such a surface is by no means trivial and accuracy of results decays anyway.

3.3 Co-energy and finite differences

The last approach consists in evaluating the derivative of the co-energy functional using finite differences. This technique has been proposed several times in the literature in the context of FEM approaches, but discarded in view of possible cancellation errors, of the difficulty intrinsic in the evaluation of the co-energy of the infinite domain and of the need of multiple analyses. All these obstacles seem to play a minor role with the present BEM-FEM approach and finite differences turn out to be very competitive both in terms of accuracy, as shown in Section 4, and in terms of efficiency. Indeed, co-energy

is a global measure and suffers marginally from the presence of local narrow gaps; moreover the analysis of industrial components is often required for a series of positions of Ω_{FM}, so that finite differences can be computed at almost zero cost. Even if a single geometric configuration is needed, the second phase, which is necessary for computing the finite difference, can be performed employing the relative permeability η_r obtained at convergence and the global cost hence gets only marginally incremented.

Let us consider the co-energy of the infinite domain, making a distinction between linear and non linear parts:

$$\Psi = \int_{\Omega_F} \int_0^{\mathbf{H}} \mathbf{B} \mathrm{d}\mathbf{H} \mathrm{d}V + \frac{\mu_0}{2} \int_{\Omega_A} (\nabla\phi^p + \mathbf{H}^a) \cdot (\nabla\phi^p + \mathbf{H}^a) \mathrm{d}V \quad (17)$$

The first term can be directly computed from the solution of eqns. (6) and (7). Focusing on the latter, we first remark that:

$$\int_{\Omega_A} (\nabla\phi^p \cdot \nabla\phi^p + 2\nabla\phi^p \cdot \mathbf{H}^a) \mathrm{d}V = \int_\Gamma \phi^p (B_n + B_n^a) \mathrm{d}S$$

where $B_n^a = \mu_0 \mathbf{H}^a \cdot \mathbf{n}$. Moreover:

$$\frac{\mu_0}{2} \int_{\Omega_A} |\mathbf{H}^a|^2 \mathrm{d}V = \Psi_\infty^a - \frac{\mu_0}{2} \int_{\Omega_F} |\mathbf{H}^a|^2 \mathrm{d}V$$

where Ψ_∞^a of the co-energy in the infinite domain if $\mu_r = 1$ in Ω_F.

Hence, finally

$$\Psi = \int_{\Omega_F} \left(\int_0^{\mathbf{H}} \mathbf{B} \mathrm{d}\mathbf{H} - \frac{\mu_0}{2} |\mathbf{H}^a|^2 \right) \mathrm{d}V + \frac{1}{2} \int_\Gamma (\phi - \phi^a)(B_n + B_n^a) \mathrm{d}S + \Psi_\infty^a \quad (18)$$

Clearly, when computing finite differences, Ψ_∞^a cancels out since the current is assumed to be independent of Ω_{FM} movements.

4 Numerical examples

4.1 Levitating sphere

Let us consider the classical benchmark of a hollow sphere with center point in $(0,0,0)$, outer radius 50 mm, inner radius 35 mm, $\mu_r = 500$, immersed in the magnetic field created by a circular coil of radius 70 mm and lying in a plane $x_3 = 30$ mm with given input current $I = 20000$ A.

Table 1 : Comparison of forces [N] on hollow sphere with different techniques

Mesh	Mx	MxS	FD1	FD2
M1	332.7	332.4	342.87	343.02
M2	358.9	354.5	359.4	359.5
M3	370.9	362.8	365.6	365.7
M4	372.0	370.18	370.99	371.12
exact	372.88			

Four meshes (M1 with 1186 FE elements and 384 BE elements; M2 with 2813 FE elements and 864 BE elements; M3 with 6276 FE elements and 1536 BE elements; M4 with 29098 FE elements and 4707 BE elements) and four different techniques are employed for evaluating the global vertical force: *Mx* employs Maxwell tensor on S_M eqns. (15) and (16); *MxS* still applies Maxwell tensor but on $\partial\Omega_{FM}$ eqns. (13) and (14). *FD1* and *FD2*, on the contrary, are finite differences techniques using a vertical fictitious displacement of 0.001 mm 0.0001 mm respectively. A good convergence towards the exact value is observed, even with the first three very coarse meshes. The high accuracy of the *MxS* technique on the third and fourth meshes, however, has been obtained with an "optimal" surface S_M placed at a distance from Γ of the same order of magnitude as the typical surface element size. The finite difference technique turns out to be almost insensitive to the entity of the translation in a large range, numerical cancellations are virtually absent with the values of translations adopted and is hence a very robust approach.

4.2 Electromagnetic actuator

A second academic example is addressed in order to test the efficiency of the proposed approach in the presence of narrow gaps. The simple electromagnetic actuator of Figure 1 is analysed. It consists of an inner cylindrical core of length 100 mm and radius 20 mm, an external hollow cylinder of length 100 mm and width 5 mm, surrounded by a solenoidal winding simulated by 50 circular wires with a gap of 1 mm w.r.t. the cylinder surface and carrying an input current of $I = 2$ A each. The overlap between the two cylinders is of 50 mm. The material of the cylinders is assumed linear with $\mu_r = 500$.

Table 2 : Comparison of forces [N] on the inner core for different gaps between the two cylinders

gap	MxS	FD	Maxwell 2D
2 mm	.00192	.00222	.00223
1 mm	.00224	.00244	.00242
.5 mm	.00212	.00251	.00253
.1 mm	.00235	.00259	.00261

The gap between the cylinders is decreased progressively from 2 mm to .1 mm.

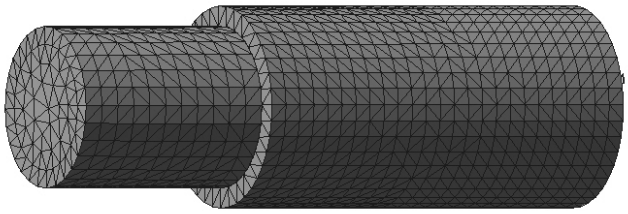

Figure 1 : Coaxial cylinders of Electromagnetic actuator: mesh adopted for the BEM-FEM approach

The results obtained are presented in Table 2 and are compared with the 2D (axysimmetric) commercial code Maxwell 2D. It is well know that 2D FEM codes can predict global forces with high precision, while this is not always the case in 3D. The accuracy of the 3D BEM-FEM code with finite differences is excellent, even if the mesh adopted is rather coarse (42291 FE elements and 11640 BE elements) and the gaps very thin. A displacement of .1 mm has been employed for computing FD, but results are almost insensitive up to 1 mm. As largely expected, the accuracy of Maxwell tensor on the skin rapidly decays even if results are still acceptable from an engineering point of view. The Mx approach has not been tested in view of the difficulty of creating a separate surface in the very thin gaps considered.

4.3 Low voltage industrial breaker

Low voltage industrial breakers are used to protect electrical circuits from dangerous overloads. Particularly, magneto-mechanical relays, like the one in Figure 2, are composed of a mechanical actuator driven by a magnetic force.

The latter originates from the magnetic field induced by the electric current flowing into the line to be protected

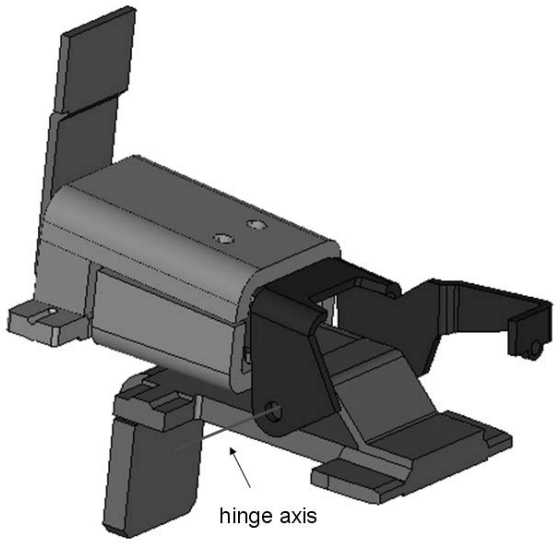

Figure 2 : Breaker with conductor and hinges

Table 3 : Comparison of moments [Nm] around the hinge axis

Mesh	Mx	MxS	FD
M1	.317	.309	.316
M2	.319	.297	.315
M3	.32	.301	.319

and is typically contrasted by a tunable spring force. The material behaviour is highly non-linear. The relative permeability is 667.7 for $|\mathbf{H}| < 238.7$ A/m and progressively decays to 1 at $|\mathbf{H}| \geq 9.54\,10^5$ A/m.

Three different meshes have been tested: M1 with 10653 FE elements and 4070 BE elements; M2 with 35079 FE elements and 9264 BE elements; M3 with 124016 FE elements and 22692 BE elements.

The upper ferromagnetic lamina (Ω_{FM}) rotates around the hinge axis as a consequence of sudden current peaks in the conductor which is placed between the two disjoint parts of Ω_F. The convergence of the non-linear procedure to a relative residuum of 10^{-3} (with respect to the rhs) is achieved in approximately 15 steps; each step requires the solution of a linear system via GMRES which converges to a relative residuum of 10^{-6} in approximately 50 iterations for the finest mesh.

The same techniques discussed for the hollow sphere in Section 4.1 have been tested here in order to evaluate the moment of magnetic forces with respect to the hinge

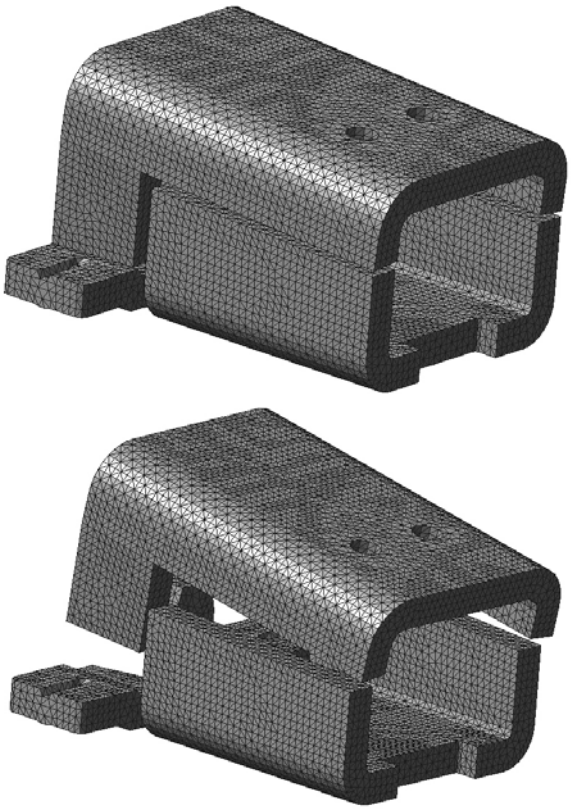

Figure 3 : Finest mesh adopted for Ω_F: original and rotated position

axis. The gaps between different parts of Ω_F still permit to create an "optimal" S_M for applying the Maxwell tensor technique. However, this nonlinear example is particularly appealing for finite differences since the second analysis (run after imposing the rotation of .001 rad to Ω_{FM} around the same axis) converges in only one step, with a virtually unchanged global cost.

The results collected in Table 3 display a very consistent behaviour of the approaches, with surprisingly small oscillations with respect to the mesh, even when applying the Maxwell tensor technique on the skin (*MxS*).

5 Conclusions

A coupled fast Boundary Element - Finite Element approach for magnetostatic problems at low frequency has been proposed, implemented and exploited for evaluating forces acting on movable ferromagnetic parts of industrial relays. The attention has been focused on two different techniques having a common energy interpretation: differentiation of co-energy and Maxwell tensor. The adoption of finite differences for evaluating the variation if co-energy has been discussed. Its robustness has been supported by three examples and competitivity with respect to alternative techniques has been pointed out, especially in the general case of non-linear material behaviour. In particular numerical cancellations have never been remarked in all the examples tested.

Acknowledgement: Support from the Italian Ministry of Education, MIUR, is kindly acknoweledged

References

Biro, O.; Preis, K.; Richter, K. (1998): Withney forms: a class of finite elements for three dimensional computation in elecretomagnetism. *IEE Proc.*, vol. 135, pp. 493–500.

Bonnet, M. (1999): *Boundary Integral Equation Methods for Solids and Fluids*. Wiley.

Bossavit, A. (1998): *Computational elecretomagnetism*. Academic press.

Chew, W.; Song, J.; Cui, T.; Velamparambil, S.; Hastriter, M.; Hu, B. (2004): Review of large scale computing in electromagnetics with fast integral equation solvers. *CMES: Computer Modeling in Engineering & Sciences*, vol. 5, pp. 361–372.

Coulomb, J. (1983): A methodology for the determination of global elecromechanical quantities from a finite element analysis and its appication to the evaluation of magnetic forces, torques and stiffness. *IEEE Transaction on Magnetics*, vol. 19, pp. 2514–2519.

Coulomb, J.; Meunier, G. (1984): Finite element implementation of virtual work principle for magnetic or electric force and torque computation. *IEEE Transaction on Magnetics*, vol. 20, pp. 1894–1896.

Frangi, A.; Faure-Ragani, P.; Ghezzi, L. (2005): Magneto-mechanical simulations by a coupled fast multipole method - finite element method and multigrid solvers. *Computers and Structures*, vol. 83, pp. 718–726.

Greengard, L.; Rokhlin, V. (1997): A new version of the fast multipole algorithm for the laplace equation in three dimensions. *Acta Numerica*, vol. 6, pp. 229–269.

Henrotte, F.; Sande, H. V.; Delige, G.; Hameyer, K. (2004): Electromagnetic force density in a ferromagnetic material. *IEEE Transaction on Magnetics*, vol. 40, pp. 553–556.

Kim, D.; Lowther, D.; Sykulski, J. (2005): Efficient force calculations based on continuum sensitivity analysis. *IEEE Transaction on Magnetics*, vol. 41, pp. 1404–1407.

Kuhn, M. (1998): The application of coupled be/fe formulations in technical magnetic field computations. *Comp. Meth. Applied Mech. Engineering*, vol. 157, pp. 193–204.

Kuhn, M.; Steinbach, O. (2002): Symmetric coupling of finite and boundary elements for exterior magnetic field problems. *Math. Meth. in Appl. Science*, vol. 25, pp. 357–371.

Melkebeek, L. V. J. (2001): A survey of magnetic force distributions based on different magnetization models and on the virtual work principle. *IEEE Transaction on Magnetics*, vol. 37, pp. 3405–3409.

Ren, Z. (1994): Comparison of different force calculation methods in 3d finite element modeling. *IEEE Transaction on Magnetics*, vol. 30, pp. 3471–3474.

Springhetti, R.; Novati; Margonari, M. (2006): Weak coupling of the symmetric galerkin bem with fem for potential and elastostatic problems. *CMES: Computer Modeling in Engineering & Sciences*, vol. 13, pp. 67–80.

Appendix A: Material derivative formulas

Let a domain Ω undergo the continuous transformation $\mathbf{y} = \mathbf{\Phi}(\mathbf{x},t)$ with associated transformation velocity $\boldsymbol{\theta}(\mathbf{x},t) = \mathbf{\Phi}_{,t}(\mathbf{x},t)$. Following classical concepts of continuum mechanics (see e.g. Bonnet (1999)) the material (or Lagrangian) derivative of a scalar or tensor function ϕ is defined as:

$$\overset{\star}{\phi} = \phi_{,t} + \nabla\phi \cdot \boldsymbol{\theta} \tag{19}$$

and yields the rate of variation of ϕ as attached to a material particle. From eqn. (19):

$$(\nabla\phi)^{\star} = \nabla\overset{\star}{\phi} - \nabla\phi \cdot \nabla\boldsymbol{\theta}$$

Analogously, for a volume integral one has:

$$I(t) = \int_{\Omega} \phi \mathrm{d}V$$
$$\overset{\star}{I}(t) = \int_{\Omega} \left(\overset{\star}{\phi} + \phi\nabla\cdot\boldsymbol{\theta} \right) \mathrm{d}V \tag{20}$$